Experimental evaluation of the stress-strain curve by continuous indentation using different indenter shapes

Jean-Marc Collin, Gérard Mauvoisin, Olivier Bartier, Rochdi El Abdi, Philippe Pilvin

▶ **To cite this version:**

Jean-Marc Collin, Gérard Mauvoisin, Olivier Bartier, Rochdi El Abdi, Philippe Pilvin. Experimental evaluation of the stress-strain curve by continuous indentation using different indenter shapes. Materials Science and Engineering: A, 2009, 501 (1-2), pp.140-145. 10.1016/j.msea.2008.09.081 . hal-01006843

HAL Id: hal-01006843
https://hal.science/hal-01006843

Submitted on 14 Oct 2017

HAL is a multi-disciplinary open access archive for the deposit and dissemination of scientific research documents, whether they are published or not. The documents may come from teaching and research institutions in France or abroad, or from public or private research centers.

L'archive ouverte pluridisciplinaire **HAL**, est destinée au dépôt et à la diffusion de documents scientifiques de niveau recherche, publiés ou non, émanant des établissements d'enseignement et de recherche français ou étrangers, des laboratoires publics ou privés.

Experimental evaluation of the stress–strain curve by continuous indentation using different indenter shapes

Jean-Marc Collin [a,*], Gérard Mauvoisin [a], Olivier Bartier [a], Rochdi El Abdi [a], Philippe Pilvin [b]

[a] *LA.R.M.A.U.R., FRE CNRS 2717, Campus de Beaulieu, Université de Rennes1, 35042 Rennes Cedex, France*
[b] *L.G.2M. Université de Bretagne-Sud, Rue de Saint-Maudé, BP 92116, 56321 Lorient Cedex, France*

Experimental applications of the methodology developed for spherical indentation are proposed in this paper. Two quasi-spherical indenters with different shapes were used in order to evaluate the stress–strain curve of five steels. Although the shape of the indenter was not perfectly spherical, it was shown that models developed for spherical indentation can be used with an adequate correction. The results are in good agreement with those obtained by tensile tests. Moreover, the case of the austenitic alloy (AISI 316L) revealed the importance of sample preparation for the experimental results.

Keywords:
Spherical indentation
Stress–strain curve
Equivalent radius
Surface preparation

1. Introduction

The indentation test was developed several decades ago in order to determine certain mechanical properties. The determination of the elastic properties is based on equations deduced from the Hertz theory [1–9]. An overview of the elastic theories applied to indentation is proposed in the paper of Borodich and Keer [10]. Concerning the determination of plastic behaviour, most of the proposed methods are commonly called reverse analysis. In such an approach, the determination of the mechanical properties is based on the inversion of models deduced from numerical studies of the indentation test. Most of these methods are based on Tabor's theory [11], which introduced the representative strain [12–15]. We can however quote other methods which are not based on the Tabor theory; Kucharski and Mróz [16] use several partial unloadings in order to determine the plastic part of the indentation depth. The determination of the yield stress and the hardening parameters can be calculated from this plastic part. Nayebi et al. [17] propose to determine the yield stress and the work hardening exponent from indentation loading. However, this method can only be applied to steels with a Young's modulus of 210 GPa and a Poisson ratio of 0.3. Another way of determining mechanical properties by indentation is by the inverse analysis approach [18,19]. In this approach, an adequate algorithm is used in order to minimize the difference between experimental and simulated observable variables.

An interpretation of spherical indentation experiments and the determination of hardening law parameters was the challenge of previous papers by Collin et al. [20,21]. The first paper concerned the determination of the contact radius by using equations deduced from the Hertz theory [1]. A methodology was then proposed to deduce both the indenter deformation and the contact radius from the knowledge of indenter and sample elastic properties. The difference δ between the measured displacement and the desired one (Fig. 1) (linked to indenter deformation) is quantified by the following formula which can be applied to spherical indenters:

$$\delta = R\left(A + B\frac{P}{\pi R^2}\frac{1-\nu_i^2}{E_i} + C\frac{P}{\pi a^2}\frac{1-\nu_i^2}{E_i} + D\left(\frac{P}{\pi R^2}\frac{1-\nu_i^2}{E_i}\right)^2 + E\left(\frac{P}{\pi a^2}\frac{1-\nu_i^2}{E_i}\right)^2 + F\frac{P}{\pi R^2}\left(\frac{1-\nu_i^2}{E_i}\right)^2\frac{P}{\pi a^2}\right) \quad (1)$$

In Eq. (1), R is the indenter radius, P is the indentation load, a is the contact radius and coefficients A–F are given by $A = -1.6817.10^{-5}$; $B = 3.6242$; $C = 0.2003$; $D = -7784.7622$; $E = -15.3689$ and $F = 649.4548$. Eq. (1) is different to the one proposed in [20] in order to take into account the indenter Poisson ratio value.

* Corresponding author. Tel.: +33 2 2323 6282.
E-mail address: jean_marc.collin@yahoo.fr (J.-M. Collin).

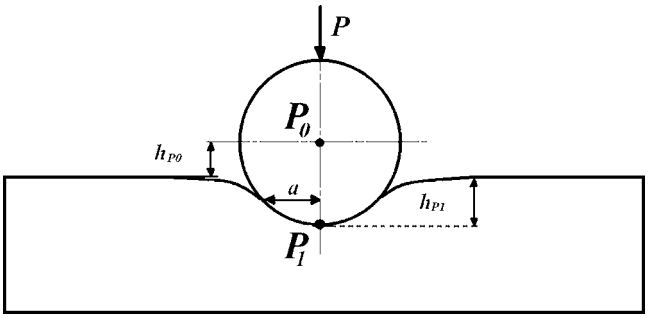

Fig. 1. Difference between measured displacement h_{P0} and wanted displacement h_{P1}.

The polynomial equation which links the contact radius a and the elastic properties of both the indenter (denoted E_i and ν_i) and the sample (denoted E_s and ν_s) can be written as

$$\alpha E_s^2 + \beta E_s + \gamma = 0, \tag{2}$$

$$\alpha = \frac{1-\nu_i^2}{E_i}\left(\frac{1-\nu_i^2}{E_i}S - 2a\right),$$

$$\beta = 2(1-\nu_s^2)\left(\frac{1-\nu_i^2}{E_i}S - a\right) - \frac{4a^2(1-2\nu_s)(1+\nu_s)}{3\pi R},$$

$$\gamma = (1-\nu_s^2)^2 S.$$

In these equations, S is the unloading slope given by $S = dP/dh$. Eqs. (1) and (2) only depend on the elastic properties of both the indenter and the sample. However, these equations can be applied in the presence of plastic deformations of the sample. Indeed, the contact radius a or the unloading slope S depend on the plastic properties of the sample. Thus, Eqs. (1) and (2) are indirectly linked to the plastic properties of the sample by the appearance of the contact radius or the unloading slope.

The second paper concerned the study of the uniqueness of the solution in the case of spherical indentation. Several models were proposed in order to describe the changes of four pieces of indentation data for power hardening law parameters. It was then shown that it is possible to deduce a quite good evaluation of the power law parameters by inversion of models. It was shown in [20,21] that isotropic hardening behaviour was not sufficient to describe the whole unloading part of the indentation curve. Then the data which can be used in the reverse analysis are the total energy W_t and the indentation load P. Our numerical analysis showed that P/E^*R^2 and W_t/E^*R^3 are well described by a power equation (E^* is the reduced Young modulus). As an example, the indentation loading curve is given by Eq. (3):

$$\frac{P}{E^*R^2} = \left(\frac{h}{R}\right)^A \exp(-B) \tag{3}$$

In Eq. (3) coefficients A and B depend on the plastic properties of the sample. The reader can refer to [21] in order to find more details about A and B. As an example, of the Hollomon law parameters (σ_y and n) and for the $P(h)$ curve, A and B are given by the following formulas using $\sigma_y^* = \sigma_y/E^*$:

$$A = \frac{0.8946 + 227.6553\sigma_y^* - 10699.6670\sigma_y^{*2} + 3.6171n + 0.0717n^2 + 1.3472n^3}{1 + 143.5716\sigma_y^* - 6922.8572\sigma_y^{*2} - 26221.0330\sigma_y^{*3} + 2.5028n}$$

$$B = \frac{5.3303 + 22.8952\sigma_y^* - 12.9210n - 7502.3214\sigma_y^{*2} + 6.2890n^2 + 18.4632\sigma_y^* n}{1 + 309.8288\sigma_y^* - 0.7235n - 4693.6406\sigma_y^{*2} - 1.9085n^2 - 303.3440\sigma_y^* n} \tag{4}$$

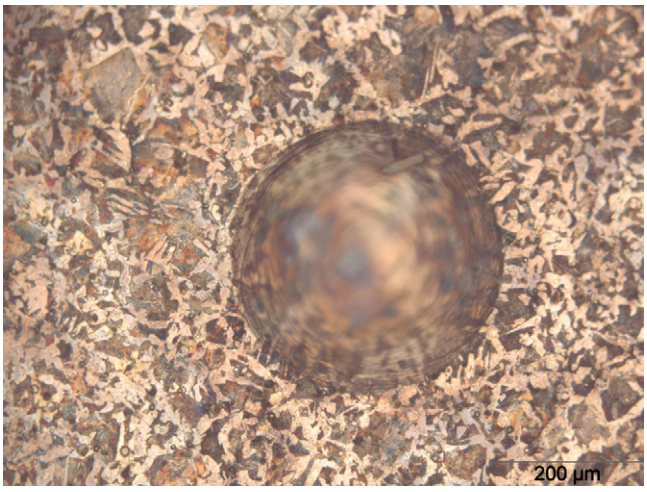

Fig. 2. Microstructure of AISI 1035.

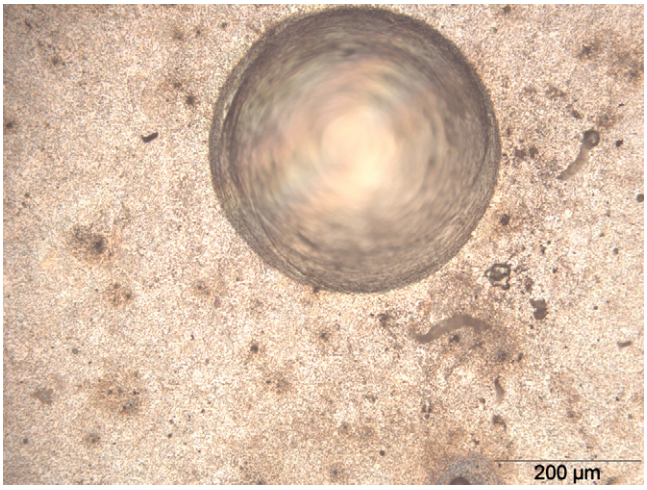

Fig. 3. Microstructure of AISI 1100.

In this paper, we propose the application of the methodology developed in [20,21] on five steels which present different kinds of microstructures. Moreover, it is shown that spherical indentation theories can be used even if the indenter has not a perfectly spherical shape.

2. Materials

In this study, five different steels were considered. Among them, four are low carbon steels: AISI 1035, 1080, 1100 and 35CrMo4. In these steels, two are composed of pearlite and ferrite phases (1035 and 35CrMo4) (Fig. 2) and two have been treated in order to transform the pearlite phase into cementite globules and ferrite (1080 and 1100) (Fig. 3). These four steels have a body-centred cubic crystal structure. The last sample is the well-known austenitic steel, AISI 316L (Fig. 4) with a face-centred cubic crystal structure.

Figs. 2–4 show the indentation imprint obtained for a load of 200 N. At this applied load, the number of metallic grains which

Fig. 4. Microstructure of AISI 316L.

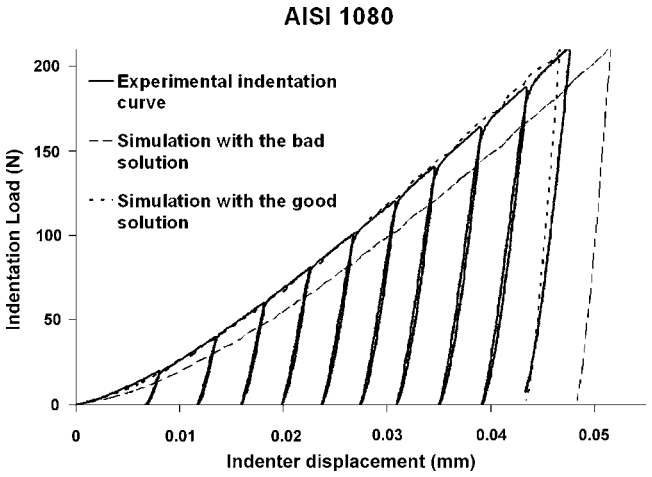

Fig. 5. Comparison between experimental and numerical indentation curves for AISI 1080.

are affected by the indentation is sufficient for considering the tested domain as representative.

The elastic properties of these samples were measured by an ultra-sound method and are close to $E = 210$ GPa and $\nu = 0.29$ for 1035, 1080, 1100 and 35CrMo4. Concerning 316L, the measured values are $E = 195$ GPa and $\nu = 0.28$. Tensile tests, realized on normalized samples issued from the same rod as the indentation samples, led to the stress–strain curve of the five steels.

3. Indenters

Indentation tests were realized on the five samples with two different indenters made of Tungsten Carbide. The first one, was previously presented in [21], and does not have a perfectly spherical shape. Thus, its profile was measured in order to simulate its behaviour. The second indenter has a sphere shape of radius $R = 1.25$ mm. The elastic properties of these two indenters were measured by ultra-sound. The Young modulus was $E_i = 590$ GPa and the Poisson ration was $\nu_i = 0.22$.

We realized indentation tests with these two indenters at 200 N and 10 loading, unloading and reloading cycles. In order to apply the spherical indentation theories to the first indenter, an equivalent radius function was determined. An indentation test was simulated with the true profile of this indenter on a fictive sample (with fixed Hollomon's law parameters). From the simulated $P(h)$ curve, the model (Eq. (3)) and the mechanical properties of the simulated sample, it was possible to determine which equivalent radius can give the same $P(h)$ curve as the simulated one. In other words, Eq. (3) was inversed with R considered as an unknown function. This led to an equivalent radius function (quoted R_{eq}) which is determined as a function of the contact radius a. This procedure can be applied to other indenters which are not perfectly spherical in order to apply spherical indentation theories. In this case, the indenter radius R has to be replaced by the R_{eq} function.

4. Experimental evaluation of the stress–strain curve by continuous indentation

It was observed that depending on the points which are considered for minimization, we can obtain a minimum with a low yield stress and a very high work hardening exponent. This phenomenon occurs if only the first points of the $P(h)$ curve are considered. It can be explained by the low deformation level at this stage which is not sufficient to describe the material's behaviour well. Fig. 5 presents the comparison between experimental and numerical $P(h_{P0})$ curves which correspond to the measured indentation curves before correction. This figure shows that the simulated $P(h)$ curve with this minimum is not close to the experimental one. We can say that, although several minima can be found, this is not a problem of non-uniqueness of the solution. This is the reason why we suggest simulating the found minimum in order to compare the experimental and numerical curves. If the two curves are close, the minimum can be considered as correct.

The procedure described in [20] has been applied to the experimental indentation curves in order to remove the displacement due to the indenter's deformations. It enabled the $P(h_{P1})$ curve (see Fig. 1) to be obtained from the $P(h_{P0})$ measured curve together with knowledge of the elastic properties of both the indenter and the sample. This procedure also allowed the contact radius changes during the indentation test to be determined. From the $P(h_{P0})$ curves, it was possible to determine the indentation data $W_t(h)$, $W_e(h)$ and $W_p/W_t(h)$. As explained in [21], $W_e(h)$ and $W_p/W_t(h)$ cannot be used in the minimization procedure as a consequence of the kinematic hardening influence. We observed that minimization with $W_t(h)$ or $P(h)$ gave almost the same results. Then, the presented results are obtained after minimization on the $P(h)$ curve.

The identification procedure was applied on the five steels and the solutions found were simulated. Figs. 6–9 present the comparison between the contact radius changes which were experimentally determined and the simulated ones for the two studied indenters. In Fig. 7, which concerns AISI1080, we can see that, for the non-spherical indenter, a difference occurs between the experimental and the numerical contact radius at the end of the indentation test. Experimental displacement is higher than that of

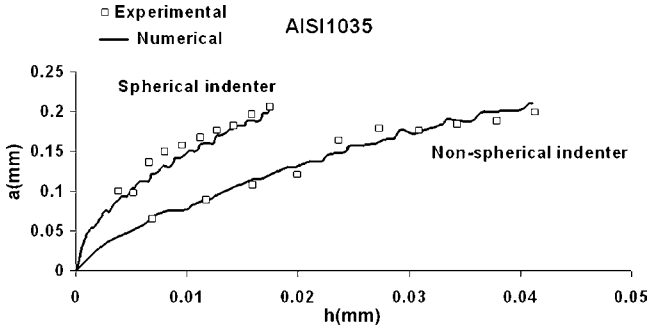

Fig. 6. Comparison between experimental and numerical $a(h)$ curves for AISI 1035.

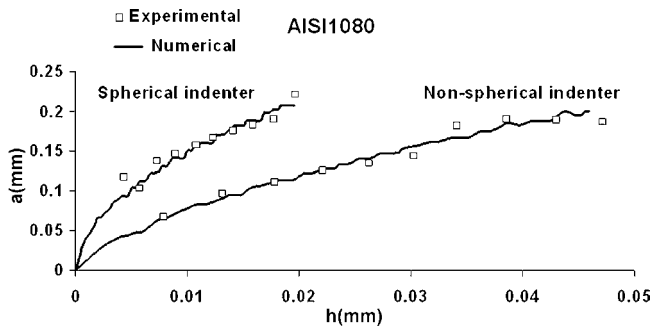

Fig. 7. Comparison between experimental and numerical $a(h)$ curves for AISI 1080.

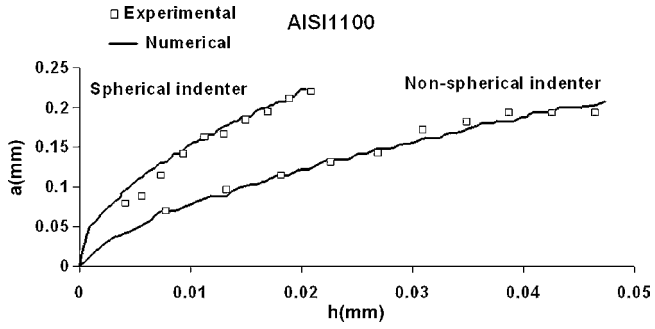

Fig. 8. Comparison between experimental and numerical $a(h)$ curves for AISI 1100.

the simulated one and the experimental contact radius is less than that of the simulated one. This is in concordance with Fig. 5 where we can observe a difference between the experimental and numerical unloading part. This difference can be explained by a variation of the elastic properties of the sample with plastic deformation. However, this aspect cannot be taken into account in the present work. Figs. 10–13 present the comparison between the identified stress–strain curves and the experimental ones for AISI1035, AISI1080, AISI1100 and 35CrMo4. In these figures, the identified parameters were obtained after minimization on the whole $P(h)$ curve. It is then shown that, for these four samples, we obtained a quite good evaluation of the stress–strain curve by continuous indentation. Moreover, the use of a non-spherical indenter with the adequate correction also gave a good evaluation of the stress–strain curve.

Concerning the austenitic steel 316L, Fig. 14 shows that this steel is very sensitive to the way the surface was polished. If this was only manually polished, the indentation displacement was much lower than if the surface was prepared with electrolytic polishing. Among the five studied samples, only 316L presents this phenomenon. This can be explained by several aspects. First of all, as this steel is not magnetic, it is impossible to rectify the indentation sample before

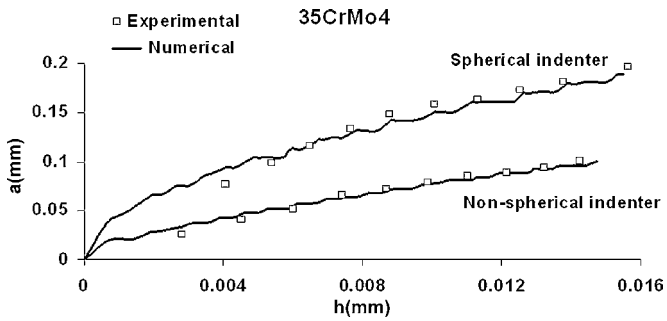

Fig. 9. Comparison between experimental and numerical $a(h)$ curves for 35CrMo4.

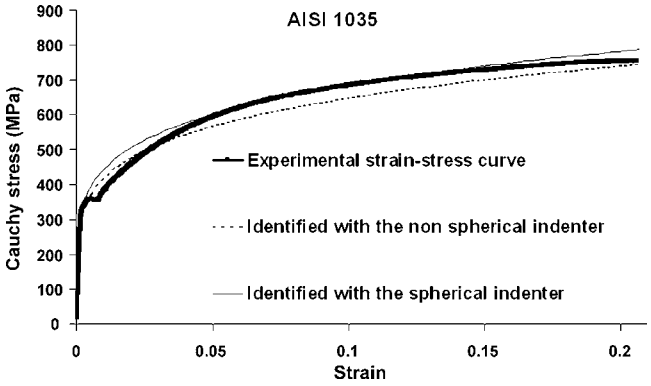

Fig. 10. Determination of stress–strain curve for AISI 1035.

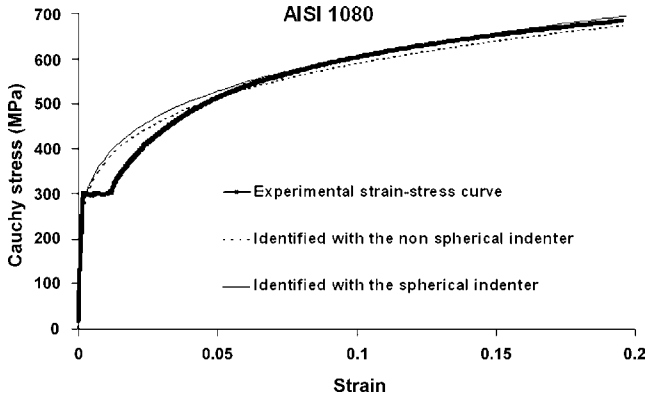

Fig. 11. Determination of stress–strain curve for AISI 1080.

polishing in order to remove the deformed coat induced by the sample machining. Moreover, Fig. 15 shows that the stress increased very quickly at the beginning of the stress–strain curve. Then, on the one hand, if we consider the yield stress as the end of the elastic area (area 1 in Fig. 15) of the curve, we obtain approximately 100 MPa. On the other hand, if we consider the commonly used yield stress at a plastic strain equal to 0.2% (area 2 in Fig. 15), we obtain approximately 400 MPa. This is the reason why electrolytic polishing was realized on the 316L indentation samples. However, this method is limited and it is not possible to remove a great depth without damaging the surface, particularly the planarity.

Fig. 16 shows the application of our methodology on 316L steel with manual and electrolytic polishing. We can see that the results

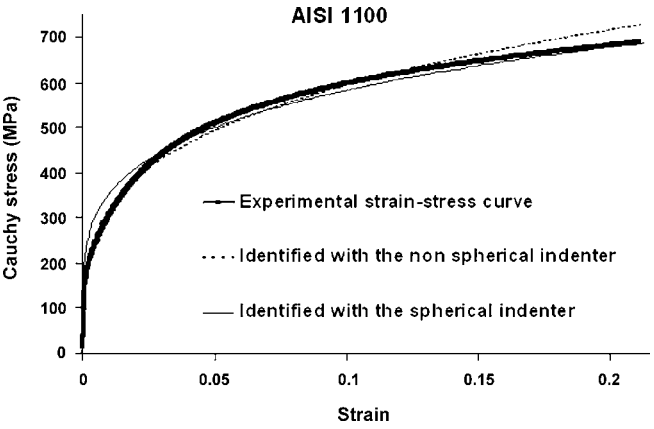

Fig. 12. Determination of stress–strain curve for AISI 1100.

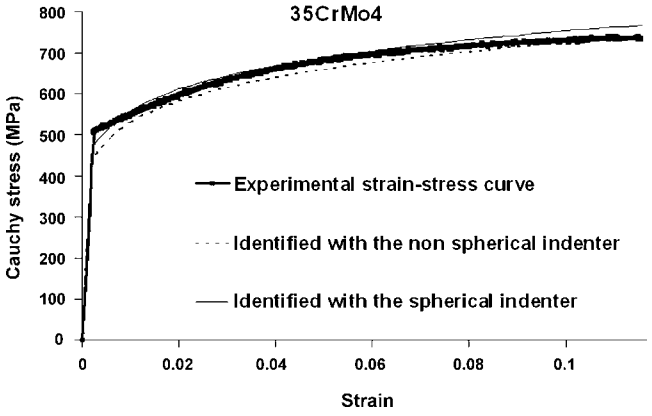

Fig. 13. Determination of stress–strain curve for 35CrMo4.

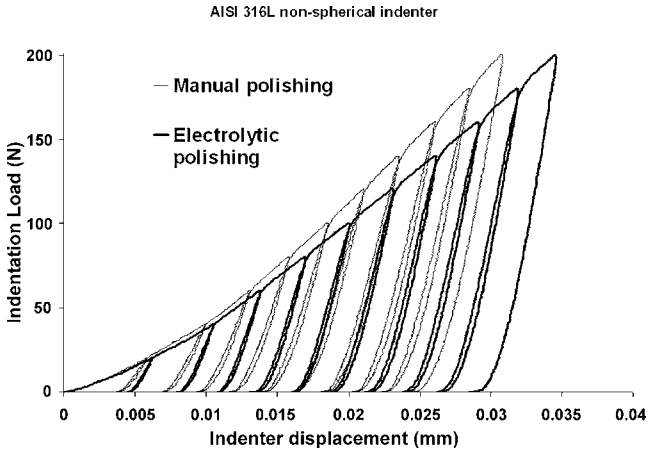

Fig. 14. Influence of polishing on the indentation curve for AISI 316L.

obtained from the sample which was manually polished are higher than the experimental stress–strain curve. Concerning the electrolytic polished sample, we can observe that the results are nearer to the experimental stress–strain curve. However, electrolytic polishing seemed not to have removed the entire deformed coat on the surface of the sample. This example, which does not work as well as the four other samples, shows the importance of the preparation of the indentation sample.

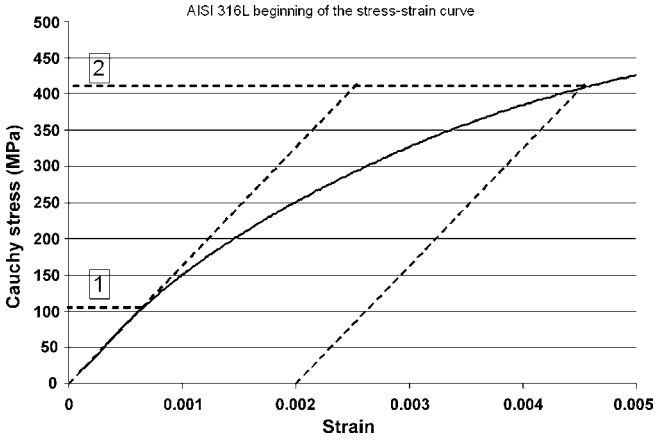

Fig. 15. Beginning of the stress–strain curve of AISI 316L.

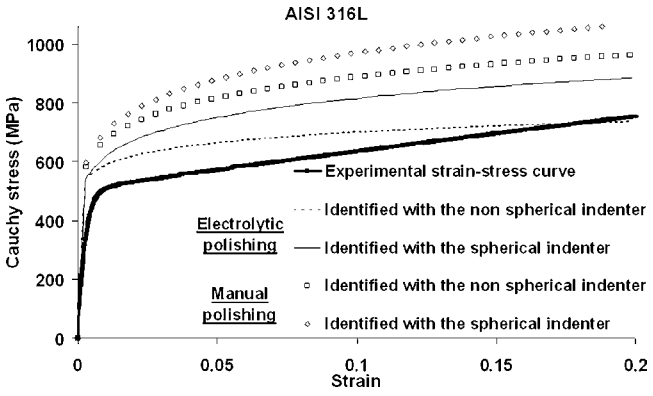

Fig. 16. Determination of stress–strain curve for AISI 316L.

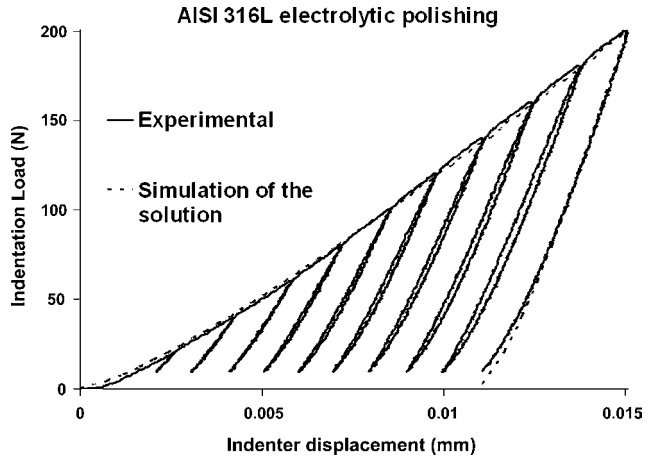

Fig. 17. Comparison between experimental and numerical indentation curve for the steel AISI 316L.

As a conclusion, the investigation on the five studied materials shows that the indentation test can provide a quite good evaluation of the stress–strain curve. The results are in good agreement with the tensile tests for low carbon steels which can be rectified and do not present a high hardening level for low deformations. Concerning the 316L steel, the results obtained by indentation cannot be considered as incorrect. Indeed, the simulation is in good agreement with the experimental indentation curve (Fig. 17 for the spherical indenter). In this case, the indentation test shows that the surface of the sample is not representative of the tensile test sample.

Thus, if the aim of the indentation test is to have a good assessment of the strain–stress curve, an adequate preparation of the surface is required. However, if the aim of the test is to characterize the material's properties at a localized area, Figs. 14 and 16 show that different indentation curves lead to a different stress–strain curve. A comparison with the stress–strain curve obtained by a tensile test can determine how much the surface was hardened.

5. Conclusion

An experimental evaluation of the spherical indentation theories developed in [20,21] was performed on five different steels. It is shown that these theories can be applied in order to obtain a good evaluation of the stress–strain curve even if the indenter does not have a perfectly spherical shape. We then propose the methodology in order to correct the indentation curve obtained with non-spherical indenters. This procedure is not restricted to

our indenter, as it can be applied to other indenters. However, it required a good knowledge of the indenter profile. Moreover, the results presented in this paper are not restricted to our models. Methods cited in the first paragraph can be applied with non-spherical indenters with the adequate correction function.

It is also shown that, for some cases, the preparation of the sample surface has a great influence on the results. For samples which can be polished manually after machining quite accurate results can be obtained. However, for the steel AISI 316L, electrolytic polishing gives better results.

Acknowledgment

This research was sponsored by the Region of Brittany.

References

[1] H. Hertz, Z. Reine Angew. Math. 92 (1882) 156–171.
[2] L.A. Galin, J. Appl. Math. Mech. (PMM) 10 (1946) 425–448.
[3] I.N. Sneddon, Int. J. Eng. Sci. 3 (1965).
[4] S.I. Bulychev, V.P. Alekhin, Zavod Lab. 41 (1975).
[5] M.Kh. Shorshorov, S.I. Bulychev, V.P. Alekhin, Sov. Phys. Dokl. 26 (1982).
[6] M.F. Doerner, W.D. Nix, J. Mater. Res. 1 (1986).
[7] J.L. Loubet, J.M. Georges, G. Meille, ASTM STP 889, 1986.
[8] W.C. Oliver, G.M. Pharr, J. Mater. Res. 7 (6) (1992) 1564–1583.
[9] J.C. Hay, P.J. Wolff, J. Mater. Res. 16 (5) (2001) 1280–1286.
[10] F.M. Borodich, L.M. Keer, Int. J. Solids Struct. 41 (2004) 2479–2499.
[11] D. Tabor, Hardness of Metals, Clarendon Press, Oxford, 1908.
[12] M. Dao, N.K. Chollacoop, J. Van Vliet, T.A. Venkatesh, S. Suresh, Acta Mater. 49 (2001) 3899–3918.
[13] N. Chollacoop, M. Dao, S. Suresh, Acta Mater. 51 (2003) 3713–3729.
[14] Y.P. Cao, J. Lu, Acta Mater. 52 (2004) 4023–4032.
[15] H. Lee, J.H. Lee, G.M. Pharr, J. Mech. Phys. Solids 53 (9) (2005) 2037–2069.
[16] S. Kucharski, Z. Mróz, Int. J. Mech. Sci. 49 (11) (2007) 1238–1250.
[17] A. Nayebi, R. El Abdi, O. Bartier, G. Mauvoisin, Mech. Mater. 34 (4) (2002) 243–254.
[18] T. Nakamura, T. Wang, S. Sampath, Acta Mater. 48 (2000) 4293–4306.
[19] G. Bolzon, G. Maier, M. Panico, Int. J. Solids Struct. 41 (2004) 2957–2975.
[20] J.M. Collin, G. Mauvoisin, R. El Abdi., Mech. Mater. 40 (2008) 401–406.
[21] J.M. Collin, G. Mauvoisin, P. Pilvin, R. El Abdi, Mater. Sci. Eng. A 488 (2008) 608–622.